Microgravity and low muon radiation affect viral pathogenesis and physiology in *Caenorhabditis elegans*

Ana Villena-Giménez,[1] Victoria G. Castiglioni[1], Esmeralda G. Legarda[1], Juan C. Muñoz-Sánchez,[1,2], Rubén González[3], Santiago F. Elena[1,4]

[1]Instituto de Biología Integrativa de Sistemas (CSIC-UV), Paterna, 46980 Valencia, Spain
[2]Department of Theoretical Physics, Universitat de València, Burjassot, 46100 Valencia, Spain
[3]Institute Pasteur, 75015 Paris, France
[4]Santa Fe Institute, Santa Fe, NM 87501, USA

E-mail: santiago.elena@csic.es

ORCIDs:
A.V.G.: 0009-0000-3564-4293
V.G.C.: 0000-0001-9884-2537
E.G.L.: 0000-0002-8560-8407
J.C.M.S.: 0000-0002-5570-4983
R.G.: 0000-0001-9588-1127
S.F.E.: 0000-0001-8249-5593

ABSTRACT

Spaceflight exposes organisms to unprecedented environmental stresses, including microgravity and reduced muon radiation. These conditions are known to impact immune functions, potentially influencing the severity of viral infections. This study investigates the effects of microgravity and below-background radiation (*i.e.*, reduced muon radiation flux) on Orsay virus infections in *Caenorhabditis elegans*. We assessed *C. elegans* fitness-related and developmental traits under a fully factorial combination of standard or microgravity with standard or below-background radiation conditions. Our findings reveal that microgravity and below-background radiation affect fecundity, with significant negative impacts on reproductive success and developmental abnormalities in infected animals. Additionally, the interaction between these environmental factors and viral infection led to complex effects on viral accumulation, which were increased under below-background radiation but reduced in microgravity. These results provide new insights into the interplay between abiotic stresses and viral infections in space, emphasizing the need for further research on the long-term impacts of spaceflight on immune function and pathogen-host interactions.

INTRODUCTION

Spaceflight conditions expose organisms to unique environmental challenges, such as microgravity (μG) and altered radiation conditions. These conditions have been shown to impose stress, affecting overall health and the immune system. In short-duration spaceflights (between 10 and 15 days), blood samples from astronauts showed altered levels of leukocyte distribution and cytokine production and a decrease in the function of Epstein-Barr virus specific $CD8^+$ T cells[1]. In long-duration spaceflights (6 months) it was reported that immune alterations persisted, finding a reduction in general T-cell function[2], impairment of natural killer cells function[3] and elevated levels of salivary antimicrobial proteins[4]. Moreover, reactivation of latent herpesviruses is a well-documented phenomenon in astronauts[4-6]; it has been reported that infections caused by Epstein-Barr virus, varicella-zoster virus and cytomegalovirus increased in frequency, duration and amplitude in long-duration versus short-duration space missions[5,7].

The composition of radiation in space largely differs from the one on Earth's surface. One of the radiation components that differs between space and Earth's surface is the muon —a charged elementary particles produced when pions decay following cosmic ray interactions with atmospheric molecules. Muons are the main cosmic radiation at sea level, with about 600 muons crossing a human body every minute[8]. As an important source of radiation for living beings, cells have developed mechanisms that buffer muon's detrimental effects[9,10]. In contrast, the muon flux is greatly reduced in space due to the absence of an atmosphere to generate them. This difference is pertinent to the radiation hormesis model, which hypothesizes that organisms respond

positively to low doses of radiation, while deviations —either increases or decreases- from these levels can be detrimental[11].

Caenorhabidits elegans is an appropriate model to study responses to a variety of stresses that can be hard to unravel in more complex organisms. *C. elegans* is a well-characterized metazoan that has been widely employed since its introduction by Sydney Brenner in the 1970s[12]. As a model organism, it has many advantages: easy visualization, fast development, a complete characterized cell lineage and genome, and an estimated genetic homology of ~80% of the protein-coding genome with humans[13]. *C. elegans* is exposed to fluctuating environmental conditions in its natural environment, such as heat, cold, food scarcity, oxygen levels, and osmotic perturbations. While repeated mild heat-shock treatments extend *C. elegans* lifespan[14], moderate treatments impair fecundity[15] and embryogenesis[16], and severe treatments decreases longevity[17]. These heat-shock phenotypic alterations are synchronized with a strong change in the transcriptional response[18]. Exposure to other abiotic stresses, such as hypertonic environments induce transcriptional responses that mimic infection response to a variety of pathogens[19] and heat shocked animals have increased survival upon exposure to *Staphylococcus aureus*[20]. In contrast, animals fed with pathogenic bacteria[21] or infected with virus[22] show an increased resistance to heat shock and ubiquitin ligases involved in the intracellular pathogen response (IPR) promote thermotolerance in order to cope with proteotoxic stress, unveiling the close link between biotic and abiotic stresses[23].

C. elegans has long been used as a model in immunity. It can regulate immune responses indirectly, often through the nervous system, by recognizing pathogens, influencing the body's development, and controlling avoidance behavior[24]. Although there are significant differences with the immune system of mammals, some mechanisms used to limit pathogenesis show remarkable phylogenetic conservation, such as uridylation and RNAi pathways[25,26]. Since the discovery of Orsay virus (OrV), a lot of effort has been put into the characterization of virus-host interaction dynamics. OrV is a bipartite positive-sense single-stranded RNA virus related to the *Nodaviridae* family that infects *C. elegans* intestinal cells[27]. Viral infection produces mild intestinal symptoms such as changes in cytoplasm viscosity, nuclear degeneration and cellular fusion[27], while mild effects in progeny production where only observed in a more susceptible strain[26]. Links between viral infection and abiotic stresses have been described in the worm, with heat stress reducing the worm's susceptibility to OrV[28] and, conversely, OrV-infected animals showing an increased tolerance to heat-shock[22].

Finally, the effect of below background radiation (BBR) environments and μG on *C. elegans* and other model organisms has been explored before. Van Voorhies *et al*. carried out phenotypic and transcriptomic studies in *C. elegans* at the underground laboratory at the Waste Isolation Pilot Plant (New Mexico, USA)[29]. Animals had faster larval growth rates, higher egg laying rates and a different gene expression profile, both at 72 h after being at BBR and after 10 generations[29].

Moreover, a reduction in fertility has been observed in *Drosophila melanogaster* flies reared at the Gran Sasso Underground laboratory (Italy)[30]. Studies in simulated μG conditions in *C. elegans* have reported no reproductive and lifespan changes in nematodes[31], increased intestinal barrier permeability[32] and induction of oxidative stress and dysregulated antioxidant machinery[33].

In this study, we have explored the role of two spaceflight-associated stresses on the outcome of a viral infection. To do so, we have studied the *C. elegans*/OrV pathosystem under a factorial combination of two abiotic factors: gravity intensity (standard and μG) and muon radiation flux (standard and BBR). We have measured different fertility traits as a proxy to the animal's fitness, and body length and morphology to identify developmental impairments. In addition to the pertinent statistical analyses, the data was fitted to a fertility model and different parameters associated to prezygotic (early oocyte development, maturation and fertilization rates) and postzygotic (abortion rate) effects estimated. We also assessed intestinal barrier permeability to determine the functional state of the intestine under these stresses, since OrV infects intestinal cells and intestinal collagens are involved in preventing viral entry[34]. Finally, we quantified OrV genomic RNA2 accumulation as a proxy to viral fitness under these different stress conditions.

RESULTS

Fecundity traits are affected by spaceflight conditions and OrV infection

We performed time-series measurements of three fecundity-related traits (number of viable progeny A, number of unfertilized eggs U, and number of nonviable embryos N) in standard environmental conditions, μG conditions, BBR conditions, and in a combination of μG plus BBR conditions (Fig. S1). These measurements were done both in non-inoculated animals (control; blue lines and symbols) and in OrV-inoculated ones (OrV; green lines and symbols). All these data were fitted to the generalized linear mixed model (GLMM) described in the Methods section. The results from these analyses are shown in Table 1. For a detailed description of the effect of the different stresses on A, U and N, we refer to the supplementary text in Supplementary Materials online. Here, we will focus on the combination of these three traits into a more eco-evolutionary relevant one, the reproductive success defined as $R = A/(A + N + U)$ (Fig. 1). We found that differences in gravity intensity had a significant effect, though of small magnitude (Table 1; $P < 0.001$, $\eta_P^2 = 0.022$), with animals reared at standard gravity having an average R of 0.950 ±0.005 that was reduced to 0.927 ±0.004 in μG. The effect of muon radiation flux was conditional to the value of gravity intensity (Table 1; $P = 0.002$, $\eta_P^2 = 0.016$). In μG, R was not affected by differences in muon radiation flux (*post hoc* test, $P = 0.691$). However, in standard gravity conditions the quasi-elimination of muon radiation flux was associated with a reduction in average R from 0.962 ±0.007 to 0.939 ±0.006 (*post hoc* test, $P < 0.001$).

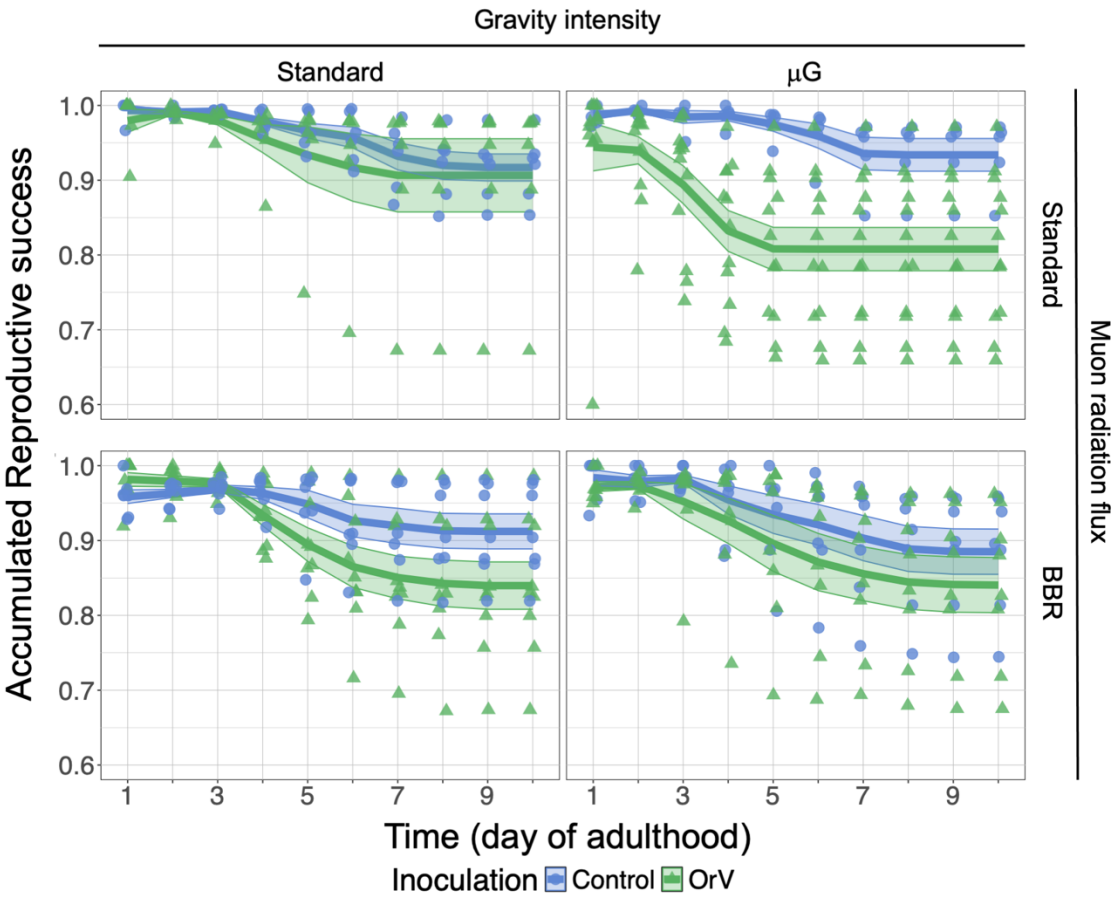

Figure 1. Reproductive success of OrV-inoculated (green) and non-inoculated (blue) animals under different combinations of spaceflight stresses. Color triangles and circles represent replicates and solid lines the mean of replicates with ±1 SEM plotted as a ribbon. Number of non-inoculated animals (sample size): n = 6 for standard conditions, n = 5 for µG, n = 7 for BBR, and n = 7 for µG and BBR. Number of inoculated animals (sample size): n = 6 for control conditions, n = 12 for µG, n = 9 for BBR, and n = 8 for BBR plus µG.

R was also negatively affected by infection itself (Table 1; $P < 0.001$, $\eta_P^2 = 0.074$), with inoculated animals having grand mean *R* of 0.917 ±0.004 and non-inoculated animals of 0.961 ±0.005, an effect of moderate magnitude. The effect of inoculation was mediated by gravity intensity (Table 1; $P < 0.001$, $\eta_P^2 = 0.024$). While *R* for non-inoculated animals was indistinguishable for both gravity conditions (0.960 ±0.006 in standard *vs* 0.961 ±0.007 in µG; *post hoc* test, $P = 0.889$), the mean *R* of inoculated animals exposed to µG was significantly lower (0.894 ±0.005 *vs* 0.941 ±0.006 in standard gravity; *post hoc* test, $P < 0.001$). The effect of infection was also mediated by the muon radiation flux (Table 1; $P = 0.004$, $\eta_P^2 = 0.014$). In this case, *R* of non-inoculated animals was significantly smaller in BBR conditions than in standard ones (0.949 ±0.006 *vs* 0.972 ±0.007; *post hoc* test, $P = 0.020$), while no effect was observed for

inoculated animals (0.924 ±0.006 *vs* 0.910 ±0.006; *post hoc* test, $P = 0.088$). Finally, the effect of inoculation significantly depended on the interaction between the two environmental conditions (Table 1; $P < 0.001$, $\eta_P^2 = 0.018$). The largest effect on R was observed for inoculated animals grown under μG and standard muon radiation flux (0.866 ±0.007), while the smallest effect was seen for non-inoculated animals under the same combination of factors (0.97 ±0.01).

In conclusion from this section, both spaceflight stress conditions impacted reproductive success, though their effects varied across traits. μG reduced reproductive success, with a more pronounced effect under BBR conditions. BBR reduced reproductive success in standard gravity, but its effects were smaller or absent in μG. Overall, the combination of microgravity and BBR intensified the negative impacts on reproductive success. OrV infection negatively impacts reproductive success, especially by reducing the number of viable progeny and increasing nonviable embryos. These effects are worsened by μG but somewhat buffered by BBR, indicating that these stresses likely affect different pathways of the infection response.

The observed effects of BBR and viral infection are prezygotic

The above statistical descriptions and analyses highlight the effect of the three experimental factors in the data. However, this sort of analyses fails to provide a mechanistic explanation for the observed differences. To dig into possible mechanisms, we developed a simple model that describes the processes from the maturation of germline precursors up to the hatching of eggs to liberate L1 larvae. The model is described by the set of six ordinary differential equations given by Eqs. 1 – 6 (see Methods). The model includes five parameters to describe different processes. Fitting the data shown in Fig. 1 into Eqs. 1 – 6 allows to disentangle whether observed differences in A, N and U under different environments and infection status can be attributable to pre- or post-zygotic effects. Table 2 shows the fitting estimates for each condition (see Fig. S2 for illustration of the best fittings). Table S1 shows the results of the three-ways ANOVA model fitted to the parameter estimates. Gravity intensity itself had no significant effect on any of the six model parameters. Muon radiation flux had significant effects, of large magnitude, in the rates of germline precursors differentiation into mature oocytes (δ) as well as in the rate of oocyte migration from the gonads into the spermathecae (η). Animals reared in BBR conditions experienced a reduction in both parameters, in the case of δ from 0.65 ±0.03 d^{-1} to 0.45 ±0.02 d^{-1} (*post hoc* test $P < 0.001$); in the case of η from 0.92 ±0.06 d^{-1} to 0.69 ±0.06 d^{-1} (*post hoc* test $P = 0.008$).

Infection status had a significant effect of large magnitude in δ and η (Table S1; $P < 0.001$, $\eta_P^2 \geq 0.209$ in both cases) and significant but of moderate magnitude in the initial number of germline precursors (G_0) and in spermatocyte to germline precursors initial ratio (α) (Table S1; $P \leq 0.038$, $\eta_P^2 \leq 0.107$ in both cases). Inoculated animals show a reduction in δ from 0.62 ±0.03 d^{-1} to 0.47

±0.02 d^{-1} (*post hoc* test $P < 0.001$), an increase in η from 0.65 ±0.06 d^{-1} to 0.96 ±0.06 d^{-1} (*post hoc* test $P < 0.001$), a reduction in α from 0.92 ±0.02 to 0.86 ±0.02 (*post hoc* test $P = 0.016$), and an increase in G_0 from 270 ±14 to 309 ±12 (*post hoc* test $P = 0.038$).

Table S1 also shows that some of the effects involved interactions between the three environmental factors. Firstly, δ was affected by gravity intensity in a manner dependent on the muon radiation flux (significant interaction gravity by radiation term; $P = 0.006$, $\eta_P^2 = 0.138$): in standard muon radiation flux $\delta = 0.72 \pm 0.04$ d^{-1} in standard gravity intensity but reduced to $\delta = 0.58 \pm 0.03$ d^{-1} in μG (19.7% reduction; *post hoc* test $P = 0.003$); in BBR conditions $\delta = 0.42 \pm 0.03$ h^{-1} in standard gravity intensity was statistically undistinguishable from $\delta = 0.47 \pm 0.03$ d^{-1} in μG (*post hoc* test $P = 0.107$). Secondly, the magnitude of the effect of muon radiation flux on δ and η also depended on the infection status (Table S1; $P \leq 0.001$, $\eta_P^2 \geq 0.188$ in both cases). In the case of δ, non-inoculated animals reared in standard muon radiation flux conditions had $\delta = 0.78 \pm 0.04$ d^{-1}, while at BBR conditions, $\delta = 0.46 \pm 0.03$ d^{-1}, representing a significant reduction (*post hoc* test $P < 0.001$); inoculated animals grown at standard muon radiation flux conditions had $\delta = 0.51 \pm 0.03$ d^{-1}, while at BBR conditions, $\delta = 0.43 \pm 0.03$ d^{-1}, representing a significant reduction (*post hoc* test $P = 0.036$). In other words, the magnitude of the effect on δ due to muon radiation flux was larger in non-inoculated animals than in inoculated ones (41.6% *vs*. 15.56% reductions). In the case of η, non-inoculated animals reared in standard muon radiation flux had $\eta = 0.6 \pm 0.1$ d^{-1}, while at BBR conditions, $\eta = 0.68 \pm 0.08$ d^{-1}, values that were not significantly different (*post hoc* test $P = 0.315$); inoculated animals grown at standard muon radiation flux conditions had $\eta = 1.22 \pm 0.08$ d^{-1}, while at BBR conditions, $\eta = 0.70 \pm 0.08$ d^{-1}, representing a significant reduction (*post hoc* test $P < 0.001$). In other words, the magnitude of the effect on η due to muon radiation flux was larger in inoculated animals than in non-inoculated ones (44.0% reduction *vs*. 9.8% nonsignificant increase).

In conclusion, we found that the three environmental factors had significant effects in parameters related to prezygotic processes, with the magnitude and sign of the observed changes depending on the precise combination of factors. In terms of wider effects, OrV infection affected more developmental processes than either muon radiation flux and gravity intensity.

Synergistic effects of μG, BBR and infection in developmental rates

After measuring the impact of spaceflight conditions and viral inoculations on fertility traits, we investigated the impact on growth. We measured the effects of μG, BBR, OrV infection, and their combinations on the growth rates of animals from L1 larvae to L4 adults (Fig. 2A). There was a significant overall effect of gravitational differences yet of small magnitude ($\chi^2 = 45.734$, 1 d.f., $P < 0.001$, $\eta_P^2 = 0.005$), with animals raised in μG being larger than those raised under standard

conditions (678 ±4 μm *vs* 640 ±4 μm). This difference increased with time post-hatching (χ^2 = 48.942, 3 d.f., $P < 0.001$; $\eta_P^2 = 0.006$). Muon radiation flux also had a significant overall effect of small magnitude (χ^2 = 28.179, 1 d.f., $P < 0.001$, $\eta_P^2 = 0.003$), with nematodes exposed to BBR conditions being larger than those in standard conditions (674 ±4 μm *vs* 644 ±4 μm). The effect magnitude was also time-dependent (χ^2 = 17.747, 3 d.f., $P < 0.001$; $\eta_P^2 = 0.002$). Inoculation had a significant impact as well (χ^2 = 20.630, 1 d.f., $P < 0.001$, $\eta_P^2 = 0.002$), with inoculated animals being smaller than their non-inoculated counterparts (647 ±4 μm *vs* 672 ±4 μm). The effect magnitude varied over time, generally increasing (χ^2 = 14.983, 3 d.f., $P = 0.002$; $\eta_P^2 = 0.002$), though not uniformly across all conditions.

The magnitude of these effects depended on the pairwise interactions of the three factors ($\chi^2 \geq 10.424$, 1 d.f., $P \leq 0.001$, $\eta_P^2 \leq 0.003$ in all combinations) and varied over time ($\chi^2 \geq 12.269$, 3 d.f., $P \leq 0.007$, $\eta_P^2 \leq 0.002$ in all combinations). Focusing first in the interaction between gravity intensity and muon radiation flux, animals grown in μG under BBR conditions were, on average, larger than those grown only in μG (702 ±6 μm *vs* 654 ±5 μm; *post hoc* test, $P < 0.001$) and larger than those grown only under BBR conditions (702 ±6 μm *vs* 646 ±6 μm; *post hoc* test, $P < 0.001$). Now looking at the interaction between gravity intensity and inoculation, we found that under standard gravity intensity, inoculated animals were on average smaller than non-inoculated ones (618 ±6 μm *vs* 671 ±4 μm; *post hoc* test, $P < 0.001$), while inoculation had no significant effect on growth under μG conditions (675 ±6 μm *vs* 673 ±6 μm; *post hoc* test, $P = 0.602$). Finally, exploring the interaction between muon radiation flux and inoculation, we observed that inoculation had no net effect on animals grown under BBR conditions (675 ±6 μm *vs* 673 ±6 μm; *post hoc* test, $P = 1$). Three-way interactions were not statistically significant either independently (χ^2 = 0.225, 1 d.f., $P = 0.636$) or over developmental time (χ^2 = 2.034, 3 d.f., $P = 0.565$), indicating that the effect of infection was independent on the interaction between the two spaceflight abiotic stresses.

Populations of *C. elegans* primarily consist of hermaphrodites, with males appearing infrequently under standard conditions, in our experiments at frequencies as low as 1 male per 1606 individuals. However, the frequency of males increased under spaceflight stresses. In μG, 4 males were observed in a population of 733 individuals. In BBR, 15 males were found out of 3490 individuals, and 5 males out of 1640 individuals were observed when raised under combined μG and BBR conditions (Fig. 2B). Neither gravity intensity (χ^2 = 2.606, 1 d.f., $P = 0.106$) nor muon ration flux (χ^2 = 1.431, 1 d.f., $P = 0.232$) alone significantly affected the number of males produced. However, the combination of these factors led to a ~5-fold increase in male frequency compared to standard conditions, a statistically significant but small effect (χ^2 = 5.315, 1 d.f., $P = 0.021$, $\eta_P^2 = 0.001$).

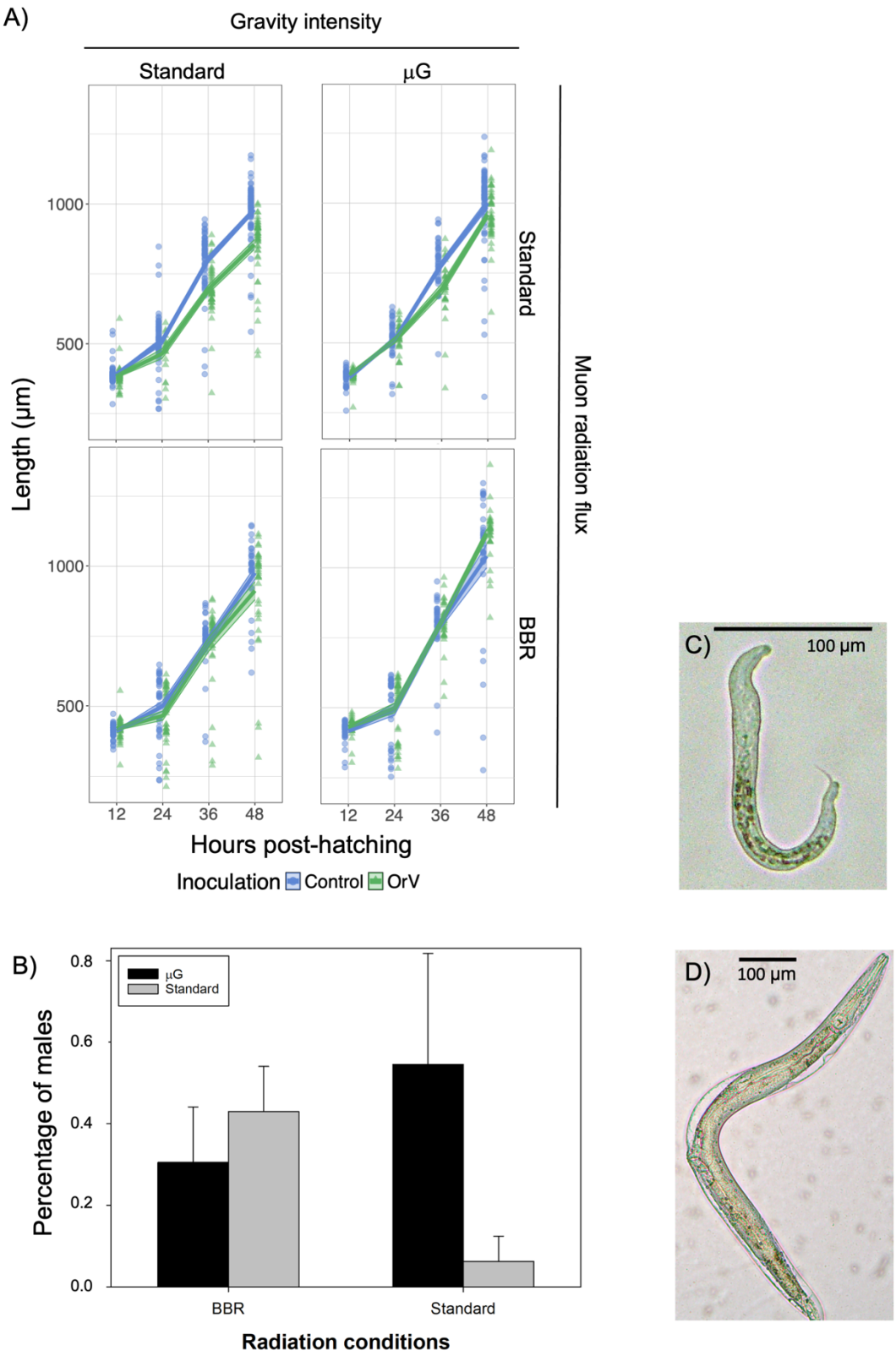

Figure 2. Growth and development of non-inoculated and OrV-inoculated animals under different gravity and radiation conditions. (**A**) Starting from plates with 400 individuals, photographs were taken at 12, 24, 36, and 48 hours after hatching to assess the effect of the stress conditions in larval development. Solid lines represent the mean and ribbons represent ±1 SEM

(number of replicates ranged from 19 to 130). (**B**) Percentage of males quantified 48 h after hatching under standard (n = 1606), μG (n = 733), BBR (n = 3490), and BBR plus μG (n = 1640). Error bars represent ±1 SEM. (**C**) Individual with bulges around the body and short length. Extracted from the population of 24 h in BBR conditions; scale bar of 100 μm. (**D**) Individual defective in molting. Extracted from the population 48 h in BBR plus μG; scale bar of 100 μm.

In addition, under BBR conditions we observed dumpy animals —characterized by a shorter and stouter body morphology due to defects in structural genes like collagens (3 in a population of 1843 individuals), as well as other rare phenotypes, which included increased head-length proportion (Fig. 2C), and body bulges molting defects (Fig. 2D). Neither of these phenotypes were observed in standard conditions (Binomial test, $P < 0.001$). A possible explanation is that lack of radiation might affect genes that are involved in molting, such as collagens[35].

In conclusion, OrV inoculation mitigates the effect of the two spaceflight-related stresses on developmental rates, the two abiotic stresses result in increased male frequency and BBR also causes diverse morphological abnormalities.

The impairment of intestinal barrier by μG is antagonized by BBR

Intestinal permeability has been shown to be affected by several abiotic stresses, including a significant increase in μG[31]. We tested the effect of gravity intensity and muon radiation flux in the intestinal permeability of animals (Fig. 3). Firstly, we observed a significant overall increase, of large magnitude, in permeability of animals grown in μG conditions (χ^2 = 15.882, 1 d.f., $P <$ 0.001, η_P^2 = 0.187), as previously reported. Conversely, BBR conditions were associated to a reduction, of moderate magnitude, in permeability (χ^2 = 8.387, 1 d.f., P = 0.004, η_P^2 = 0.099). No significant interaction between the two factors has been found (χ^2 = 0.461, 1 d.f., P = 0.497), suggesting that permeability alterations are a consequence of overlapping mechanisms.

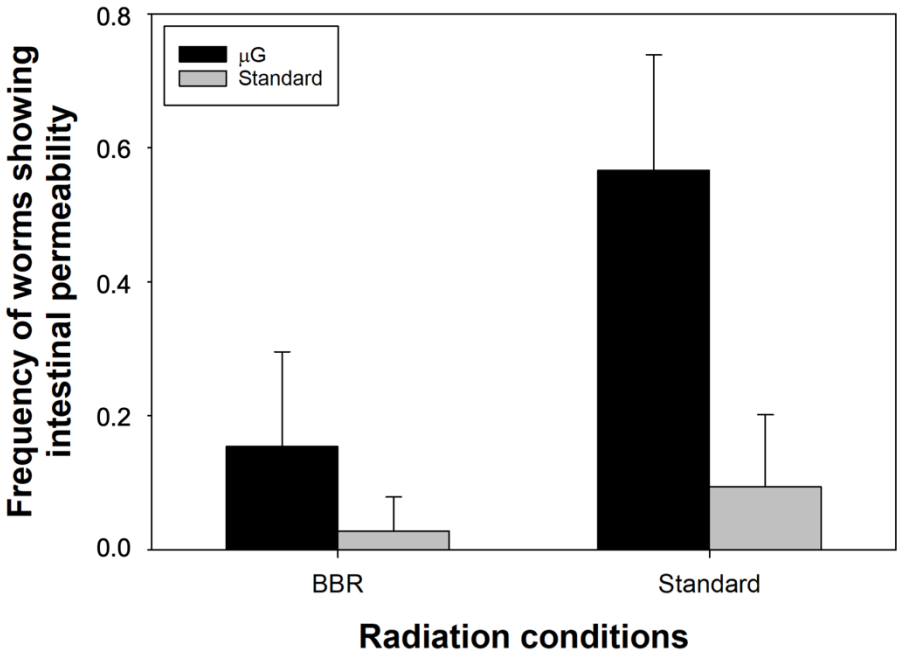

Figure 3. Intestinal permeability of animals under standard gravity (n = 30), μG (n = 28), BBR (n = 34) and μG plus BBR (n = 24) conditions. Synchronized L1 animals were grown at 20 ºC during 48 h and then fed with a solution containing erioglaucine disodium for 3 h. Nematodes showing blue staining outside the intestinal tube were scored as permeable whether the salt diffused throughout the body or leaked out. Error bars represent ±1 SEM.

Viral accumulation dynamics are strongly affected by differences in gravity intensity and the flux of muons

Finally, in an effort to characterize the interactions between the two spaceflight conditions and the viral infection, we followed the progression of OrV viral load throughout the whole larval development of inoculated animals. We have previously shown that in standard conditions, OrV infection follows two waves of viral load from L1 larvae to sexually mature adults[36]. A first peak is reached approximately 12 hours post-inoculation (hpi) in L1 larvae, which is followed by a sharp decline as antiviral responses are activated by the developing animals, reaching a minimum approximately 18 – 20 hpi (L2 larvae). From there on, a second wider peak is reached that last for at least 18 additional hours (L3 larvae and L4), afterwards, viral load is low yet viral replication continues at low levels[35]. This pattern is in agreement with our data in standard conditions of gravity and muon radiation flux (Fig. 4, upper left panel).

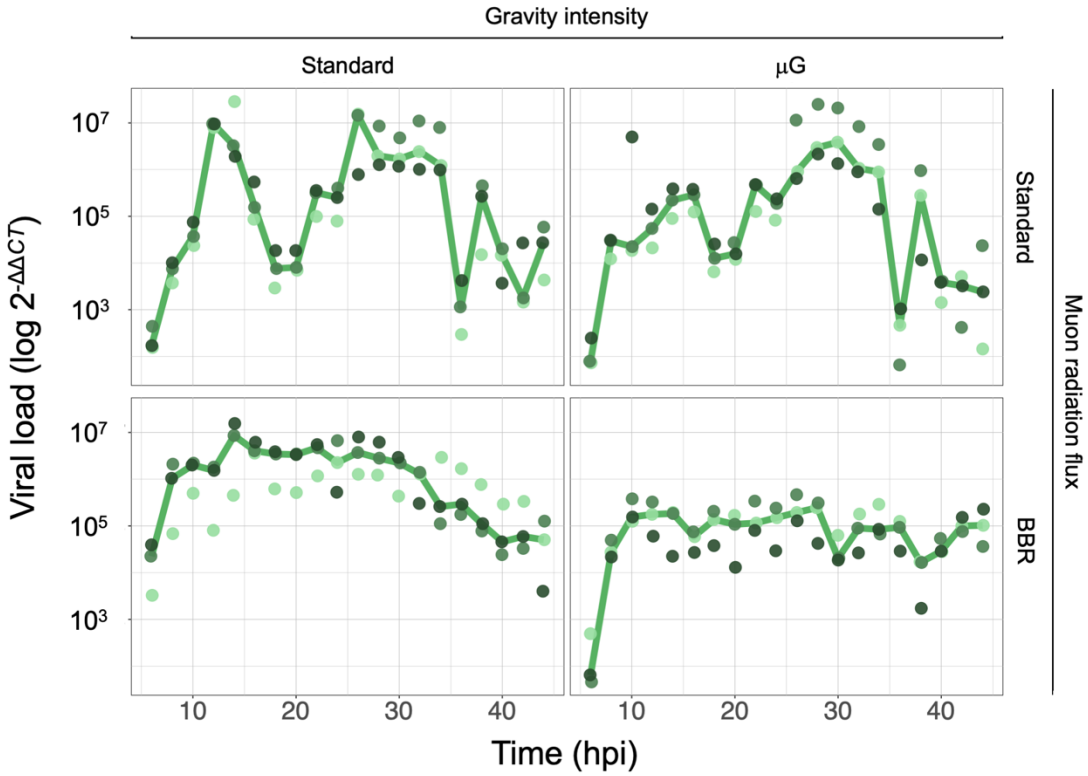

Figure 4. Log-fold change of OrV accumulation, relative to the expression of housekeeping gene *cdc-42*, evaluated in inoculated animals reared under the indicated combination of gravity intensity and muon radiation flux conditions. Different green tones represent independent biological replicates (pools of ~300 animals per time point). The solid line represents the mean trajectory.

Gravity intensity and muon radiation flux conditions had effects of opposite sign on viral load dynamics. The grand mean viral load measured in µG conditions was $(5.69 \pm 0.05)\cdot 10^4$, lower than the $(2.53 \pm 0.02)\cdot 10^5$ in standard gravity conditions, representing significant yet of small magnitude effect ($\chi^2 = 2255.942$, 1 d.f., $P < 0.001$; $\eta_P^2 = 0.058$). As illustrated in Fig. 4, the effect of µG is time-dependent ($\chi^2 = 1415.456$, 19 d.f., $P < 0.001$; $\eta_P^2 = 0.037$) and consists in reducing the height of the first peak of viral load and increasing the maximum value and duration of the second (both upper panels in Fig. 4). The grand mean viral load measured in BBR conditions was $(1.87 \pm 0.02)\cdot 10^5$, compared to a value of $(7.67 \pm 0.06)\cdot 10^4$ measured in normal muon radiation flux conditions, representing a major increase in viral load ($\chi^2 = 1593.430$, 1 d.f., $P < 0.001$; $\eta_P^2 = 0.041$). The effect of BBR widely impact the temporal dynamics of OrV accumulation ($\chi^2 = 3103.138$, 19 d.f., $P < 0.001$; $\eta_P^2 = 0.080$), erasing the differences between the two peaks, as only a maximum value is reached about 12 hpi that remains constant until 36 hpi and then slowly declines (compare both left panels in Fig. 4).

The observed effects were not independent, as a significant interaction term has been found among them ($\chi^2 = 1636.075$, 1 d.f., $P < 0.001$; $\eta_P^2 = 0.042$) that was also time-dependent ($\chi^2 =$

1934.595, 19 d.f., $P < 0.001$; $\eta_P^2 = 0.050$). The combined effect of both spaceflight stresses in viral fitness shows the atypical pattern observed in BBR conditions but with a further reduction in viral load along the whole period of animal development (compare the upper left and lower right panels in Fig. 4).

Overall, μG has a negative impact on viral replication, whilst BBR has a positive one and the combination of these stresses has an even greater negative impact than by themselves. Further studies are necessary in order to determine whether these results are consequence of a disrupted cellular homeostasis, an impact of the stresses on the immune response or due to a direct effect on viral replication.

DISCUSSION

Exploring deep space is a primary aim of the modern space era. Effective countermeasures against the negative health effects of extended spaceflight must be developed. In this study we sought to investigate the independent and combined effects of two spaceflight conditions, namely microgravity (μG) and below background muon radiation flux (BBR), on the outcome and severity of a viral infection. To do so, we have used the pathosystem formed by the nematode *C. elegans* and its natural viral pathogen the OrV. We acclimatized the host to the abiotic stresses and performed the experiments in the third generation of acclimatized animals. This enables us to investigate long-term effects of microgravity and BBR in the worm since it is known that in *C. elegans* responses to stress are transmitted intergenerationally[32].

Firstly, our results confirm previous observations that both μG and BBR represent stressful environments that affect responses to viral infections[1-7] and developmental rates and fecundity[29]. Interestingly, our data show that the magnitude of these effects varied for different fecundity components and developmental rates, and that the two spaceflight stresses acted no independently. This non-independence of effects suggests that the animal's responses to μG and BBR should at least partially overlap.

The small but significant increase in male frequency suggests that spaceflight conditions may disrupt cellular homeostasis and processes as important as chromosomal disjunction could be affected by these stresses, as has been observed with other environmental stresses[37]. Furthermore, increasing the number of males could have big consequences at the population level, as increased mating increases genetic diversity in the population by promoting allele shuffling and thus bolstering adaptation to the stressful conditions[38,39].

It has been well documented that spaceflight conditions impact immune cells, including a reduced activity of T-cells and altered cytokine production[3,40]. This is consistent with previous observations in astronauts who experienced herpesvirus reactivation during spaceflight[5-7]. Our

results are congruent with these observations. μG itself has a small effect in the shape of the virus accumulation curve, yet increasing 2.7% the accumulated viral load along the 44 hpi. In contrast, BBR itself has a major effect in OrV accumulation dynamics, erasing the distinction between both viral production phases and resulting in 34.2% reduction in accumulated viral load by the end of the experiment. The result of combining both stresses fully change the temporal shape of viral production, looking it closer to the one observed at BBR, and further reduce the accumulated viral load at the end of the experiment 71.5%. These observations suggest that (*i*) the precise simulated μG conditions may be causing a minor impairment in the worm's immune system and that (*ii*) the stress induced by BBR in nucleic acids stability negatively impacts OrV replication by a mechanism still to be found.

Several studies have shown that short-term exposures to μG exert small and reversible alterations in the transcriptome of *C. elegans*, though prolonged expositions result in transgenerational reversible effects of larger magnitude[31,41,42]. Overall, these transcriptomic alterations affect longevity-regulating insulin/IGF-1[43] and sphingolipid signaling pathways[42], neuronal function and/or cellular metabolism mediated by the *daf-16*/FOXO signaling pathway[41] and misregulation of responses to oxidative stress and the antioxidant defense system[33]. Infection often leads to the generation of reactive oxygen species (ROS) as part of the immune response, which creates oxidative stress[44]. In principle, the failure to produce ROS antiviral responses would result in enhanced virus accumulation, which we have observed in the case of μG conditions.

Our study is one of the first to explore the biological implications of the absence of muon radiation flux during spaceflight on viral infection. While the majority of research has focused on cosmic radiation exposure or natural background radiation, the reduction of secondary cosmic rays, including muons, presents an underexplored variable[29]. Furthermore, no study to our knowledge has explored the effect of lack of radiation in the progression of a viral infections, despite the absence of muon radiation in space could potentially contribute to the observed viral activation in astronauts. Muon radiation has been present during organisms' evolution and they have developed mechanisms directed to cope with the effects of this type of radiation in cells genetic material integrity and physiological processes. The negative impact of lack of muons radiation in reproductive success aligns with the emerging theory of radiation as an hormetic agent[11], in which doses below and above natural background may have harmful effects for organisms. As mentioned above, our data suggest a significant increase of viral accumulation, reduced reproductive success and appearance of abnormal phenotypes in BBR compared to standard radiation. Ongoing experiments will bring to light the possible mechanisms by which BBR negatively affect virus accumulation, either as an indirect consequence of the different regulation of cellular pathways or as a direct result of the lack of radiation upon the viral replicase.

The combined impact of μG and BBR, creates a singular environment that affects viral infection dynamics. The results discussed above support the hypothesis that the stresses of spaceflight are not isolated but interact to modulate viral reactivation or replication. The immune dysregulation caused by μG, when compounded by the altered radiation environment, may increase the likelihood of viral outbreaks or the emergence of more virulent viral strains during long-duration spaceflight. For example, the reduction in DNA repair efficiency under space radiation exposure, coupled with μG-induced immune suppression, may explain the observed reactivation of herpes-like viruses[5-7]. Long-term spaceflight stresses might accelerate viral evolution, particularly in DNA viruses. The experimental data support the idea that the simulated space environment impact the dynamics of RNA virus accumulation, and ongoing work will illustrate whether the genetic variability in the OrV populations is also affected.

From our modeling approach (Table 2 and discussion thereof) has shown that the observed effects are mostly explained by differences in parameters associated with early prezygotic stages during the egg maturation to fecundation. These results are consistent with other experimental observations. Van Voorhies *et al*. showed that regulation of major sperm protein genes (MSP) was altered in BBR condition[29]. MSPs were first identified as being involved in sperm motility and is required for the sperm ameboid-like crawling[45]. MSPs are also critical in other aspects of *C. elegans* reproduction, including oocyte and egg development, ovulation, spermathecal valve dilation, and parthenogenesis[46,47]. Seeing how functionally multifaceted MSPs are, it is likely that the alteration in the expression of *msp* genes in the BBR conditions may be reflected in the prezygotic parameters of the model.

Our findings have direct implications for astronaut health during long-duration missions. The demonstrated relationship between spaceflight conditions and viral behavior underscores the need for enhanced health monitoring and countermeasures. Pre-flight viral screenings and vaccination strategies may need to be bolstered to mitigate the risks posed by viral reactivation. Moreover, therapeutic approaches that strengthen immune function or directly inhibit viral replication should be considered as part of space medicine protocols. Our study reinforces the importance of further research into the effects of the extraordinary spaceflight environment on viral pathogens. Understanding the precise mechanisms through which μG and radiation interact to influence viral infections will be crucial for developing comprehensive strategies to protect astronaut health span on future missions to Mars and beyond.

In conclusion, the experimental evidence presented in this study highlights the complex interplay between spaceflight-related stresses and viral infection. Microgravity-induced immune suppression, compounded by the absence of muon flux and the space radiation environment, creates conditions that are conducive to viral reactivation and may promote viral evolution. Our findings emphasize the need for continued investigation into the biological effects of spaceflight,

with a particular focus on viral dynamics, to ensure the safety and health of astronauts on extended missions.

METHODS

C. elegans strains and culturing

C. elegans was cultured and maintained at 20 °C on nematode growth media (NGM) agar plates seeded with *Escherichia coli* OP50. ERT54 (*jyIs8[pals-5p::GFP + myo-2p::mCherry]X*), a transgenic strain with a genetic wild-type (Bristol N2) background that expresses GFP in response to intracellular infection[48] was used for all experiments. Strain SFE2 (*drh-1(ok3495)IV;mjls228*) was used to produce OrV stocks.

In order to obtain synchronized animal populations, plates with embryos were carefully washed with M9 buffer to remove larvae and adults but leaving the embryos behind. Plates were washed again using M9 buffer after 1 h to collect larvae hatched within that time span and transferred to seeded NGM plates.

A variable number of plates of 500 synchronized L1 animals were used to assess male frequency. Plates were stored at 20 °C and, two days after hatching, males and total population were counted using a Zeiss Stemi305 stereomicroscope.

Microgravity simulation

A random position machine (RPM) (Yuri Gravity GmbH) was employed to simulate μG conditions selecting the zero-gravity mode. Values of G-force were monitored through the RPM software and maintained at approximately 0.001 – 0.002 g throughout the experiments. The RPM was placed inside an incubator at 20 ºC.

Animals used in experiments of μG conditions were acclimated along two generations, with studies done on the third generation and its progeny. Plates were sealed with parafilm to maintain their humidity.

Below-background radiation conditions

BBR experiments were performed in the LAB2400 at the Canfrac Underground Laboratory (LSC), located in the village of Estación de Canfranc (Huesca, Spain). The measured integrated muon radiation flux in this facility is ~5×10^{-3} m^{-2} s^{-1} (49). For comparison, the muon radiation flux at sea level in the Northern hemisphere is about 150 m^{-2} s^{-1} (50).

Nematodes used in BBR experiments were acclimated to this condition during two generations prior to experiments.

446 **Fertility assay**

447 L4 larvae were picked individually from a synchronized population and put in separate fresh
448 plates. Animals were transferred to fresh plates every 24 h until egg laying stopped.
449 Synchronized worm populations were inoculated after hatching. The number of nonviable (N)
450 and unfertilized eggs (U) was counted 24 h after the adult was removed from the plate to ensure
451 all eggs had hatched. Viable progeny (A) was counted 48 h after the adult was removed from the
452 plate. Reproductive success, R, was then computed as $R = A/(A + N + U)$.

453 For OrV infection experiments, a population of animals was inoculated one hour after hatching
454 with the OrV stock described below.

455

456 **Viral stock preparation, virus quantification and inoculation procedure**

457 For OrV (strain JUv1580_vlc) stock preparation, SFE2 animals were inoculated as previously
458 described[51]. In short, animals were allowed to grow for 5 days and then resuspended in M9 (0.22
459 M KH_2PO_4, 0.42 M Na_2HPO_4, 0.85 M NaCl, 0.001 M $MgSO_4$), let stand for 15 min at room
460 temperature, vortexed, and centrifuged for 2 min at 400 g. The supernatant was centrifuged twice
461 at 21,000 g for 5 min and then passed through a 0.2 μm filter. RNA of the resulting viral stock
462 was extracted using the Viral RNA Isolation kit (NZYTech). The concentration of viral RNA was
463 then determined by RT-qPCR using a standard curve, and normalized across different stocks
464 (details below). Primers used for RT-qPCRs can be found in Table S2.

465 For the standard curve, cDNA of JUv1580_vlc was obtained using AccuScript High-Fidelity
466 Reverse Transcriptase (Agilent) and reverse primers at the 3' end of the genome. Approximately
467 1000 bp of the 3' end of RNA2 were amplified using forward primers containing 20 bp coding
468 the T7 promoter and DreamTaq DNA Polymerase (Thermo Fisher). The PCR products were gel
469 purified using MSB Spin PCRapace (Invitek Molecular) and an *in vitro* transcription was
470 performed using T7 Polymerase (Merck). The remaining DNA was then degraded using DNAse
471 I (Life Technologies). RNA concentration was determined by NanoDrop (Thermo Fisher) and
472 the number of molecules per μL was determined using the online tool EndMemo RNA Copy
473 Number Calculator (https://www.endmemo.com/bio/dnacopynum.php). Primers used for the
474 standard curve can be found in Table S2.

475 For inoculation experiments, synchronized populations were inoculated by pipetting 60 μL of
476 viral stock on top of the bacterial lawn containing the animals. The normalized inoculum
477 contained $2.6 \cdot 10^7$ copies of OrV RNA2/μL. The efficiency of this viral stock (measured as
478 animals showing activation of the *pals-5p::GFP* reporter at 48 hpi) was 72 ±3 % (mean ±1 SEM,
479 n = 5 plates with 44 – 48 animals per plate).

480

481 **RNA extractions and RT-qPCRs**

482 Sample preparation and RNA extractions were performed as previously described[51].
483 Synchronized populations of 300 inoculated and control animals were collected at the designated
484 times (from 6 hpi to 44 hpi every 2 h) with PBS-0.05% Tween. Samples of inoculated animals
485 were performed in triplicates. Samples were centrifuged for 2 min at 1350 rpm and the
486 supernatant was discarded. Another two wash steps were performed before freezing the samples
487 in liquid nitrogen. 500 µL of Trizol (Invitrogen) were added to the worm pellet and the pellet was
488 disrupted by following five cycles of freeze-thawing and five cycles of 30 seconds of vortex
489 followed by 30 seconds of rest. 100 µL of chloroform were then added and the tubes were shaken
490 for 15 s and let rest for 2 min. Samples were centrifuged for 15 min at 11,000 g at 4 °C and the
491 top layer containing the RNA was then mixed with the same volume of 100% ethanol. The sample
492 was then loaded into RNA Clean & Concentrator columns (Zymo Research) and the rest of the
493 protocol was followed according to manufacturer instructions.
494 RT-qPCRs were performed using Power SYBR Green PCR Master Mix (Applied Biosystems)
495 on an ABI StepOne Plus Real-time PCR System (Applied Biosystems). 10 ng of total RNA were
496 loaded and a comparison with the endogenous gene *cdc-42* was used for relative OrV
497 quantifications. Primers used for RT-qPCRs can be found in Table S2.
498
499 **Body size measurements and analysis of abnormal phenotypes**
500 Synchronized animals were collected at 12, 24, 36, and 48 h, plates were washed with M9 buffer
501 to collect nematodes and another M9 wash was made to remove bacteria from the media. Animals
502 were mounted in a 4% agarose pad with 20% 100 mM azide and photographed using a Leica
503 Thunder DMi8 microscope with DFC9000 GTC sCMOS camera and objective HC PL APO
504 40×/0.95 CORR PH2 (Leica Microsystems). Body length was measured using the segmented
505 line tool in ImageJ[52].
506 The photographs employed to measure body size were also used to describe abnormal
507 phenotypes.
508
509 **Intestinal permeability assay**
510 The intestinal permeability assay was performed as previously described with minor
511 modifications[53]. Synchronized nematodes were washed after 48 h with S buffer (6.5 mM
512 K_2HPO_4, 43.5 mM KH_2PO_4, 100 mM NaCl) and suspended in a 1:1 solution of 1 mL of M9 buffer
513 mixed with 0.05 g of erioglaucine disodium salt (Thermo Scientific) and 1 mL of *E. coli* OP50
514 suspended in S buffer, and gently rocked for 3 h.
515 Animals were washed carefully three times with 10 mL of M9 buffer. Animals were mounted
516 on microscopic slides on top of a 4% agarose pad with 20% 100 mM azide. Photographs were
517 taken using a Leica MZ10F stereomicroscope with Flexacam C3 camera and with a Leica DMi1
518 microscope with Flexacam C1 camera. Quantifications were randomized by assigning random

names to photographs to avoid observer bias. A positive control was prepared to help us to classify the different phenotypes. Positive control was prepared by following the same assay except that animals were grown in NGM plates with 0.8 mM H_2O_2 during 48 h, as previously described[54]. Four-hundred nematodes were used in each condition.

A model of *C. elegans* fecundity and parameter estimation

Figure 5 describes a simple fecundity model for sexually mature adults at L4 developmental stage, in which a fixed number of spermatocyte cells (S) have already been produced and stored in the spermathecae. Germline precursor cells (G) differentiate into mature oocytes (O) at rate δ_G. This rate is assumed to be constant $\delta_G = \delta$ as far as germline cells exist ($G(t) > 0$) and zero otherwise. These oocytes migrate from the distal to the proximal gonads at rate η until reaching the spermathecae where, if spermatocytes are available, are fecundated with an efficiency function ψ that depends on the amount of S present in the spermatheca at time t: $\psi(S) = (1-\gamma)S/(\gamma + S) \in [0,1]$, where γ is a dimensionless parameter which modulates the value of the efficiency, resulting in fertilized and unfertilized (U) eggs. After passing through the uterus, the eggs are deposited in the agar, where, if they have been fecundated, a fraction μ will develop into L1 larvae (*i.e*, the viable progeny, A). A fraction $1 - \mu$ will stop embryonic development, resulting in nonviable embryos (N). N and U eggs will simply remain in the plates and are easily distinguishable.

Parameter	Description
δ_G	Rate of germline precursor cells differentiation
η	Rate of oocytes migration
Ψ	Fertilization efficiency
μ	Fraction of fertilized eggs viability
α	Spermatocytes to germline initial ratio

Variable	Description
G	Germline precursor cells
O	Oocytes
S	Spermatocytes
U	Unfertilized eggs
A	Viable progeny
N	Non-viable eggs

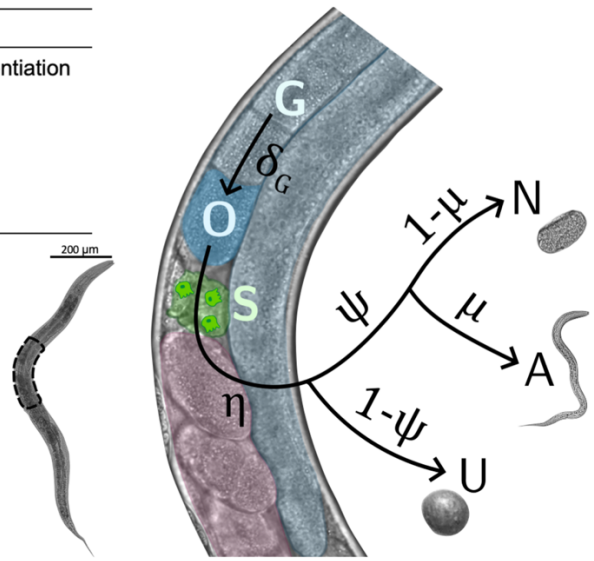

Figure 5. Parameters, variables and schematic representation of the fecundity model described by Eq. 1 – 6.

These processes can be written according to the following set of ordinary differential equations,

$$\frac{dG}{dt} = -\delta_G, \quad \text{Eq. 1}$$

$$\frac{dO}{dt} = \delta_G - \eta O, \quad \text{Eq. 2}$$

$$\frac{dS}{dt} = -\eta\psi O, \quad \text{Eq. 3}$$

$$\frac{dA}{dt} = \eta\mu\psi O, \quad \text{Eq. 4}$$

$$\frac{dN}{dt} = \eta(1-\mu)\psi O, \text{and} \quad \text{Eq. 5}$$

$$\frac{dU}{dt} = \eta(1-\psi)O, \quad \text{Eq. 6}$$

being A, N, and U are the three experimental observables (Eqs. 4 – 6). All variables were normalized by the initial number of non-differentiated germinal cells G_0. Model parameters δ, η and γ represent prezygotic stages, while μ represents a postzygotic event. Furthermore, we define the dimensionless parameter $\alpha = S_0/G_0$, which for a hermaphrodite in which the spermatocytes will be the limiting factor for asexual reproduction will be $\alpha < 1$.

We used a genetic algorithm to estimate the vector of parameters (δ, η, μ, γ, α, G_0) better fitting the experimental data for every condition. The size of the population of vectors of parameters was fixed at 600, and the number of generations was set to 10^4. The exploration of the parameter space was refined through successive generations. The cost function ($\mathcal{F}$) to minimize was the logarithm of the square sum of discrepancies:

$$\mathcal{F} = \log \sum_{i=1}^{T} \left[\left(A_i - \hat{A}_i\right)^2 + \left(N_i - \widehat{N}_i\right)^2 + \left(U_i - \widehat{U}_i\right)^2 \right]. \quad \text{Eq. 7}$$

Here, $\{t_i, A_i, N_i, U_i\}_{i=1}^{T}$ represent the experimental data obtained for T different times and $\hat{A}_i$, $\widehat{N}_i$ and $\widehat{U}_i$ denote the estimated values for the different species obtained with the mathematical model for a given set of parameters.

Within each generation, the 5% of the parameters with the lowest $\mathcal{F}$ values were designated as the elite population, remaining constant for the next generation. The next-best 80% underwent parameter crossover, while the remaining 15%, representing the least favorable parameters, experienced random mutations. The parameter space was subdivided into a logarithmic scale for parameters δ, η and γ to ensure a more balanced exploration. The model was fitted to every fertility assay data, resulting in a vector of estimated parameters per experimental replicate and condition.

Statistical analyses

Data were fitted to generalized linear mixed models (GLMM) with gravity intensity (standard *vs* μG), radiation level (standard *vs* BBR) and infection status (non-inoculated *vs* inoculated)

incorporated as fixed orthogonal factors, whereas individual animals (subjects) and days-post inoculation (repeated measures per subject) were both modeled as random factors. In the case of counts (*A*, *N* and *U*), a Poisson distribution with a log-link function was used; in the case of *R* and body size, a Normal distribution with identity-link function was used.

Intestinal permeability and the frequency of males per population data were fitted to logistic regression models using generalized linear models (GLM) with gravity intensity and radiation level incorporated as fixed orthogonal factors and assuming a Binomial distribution and a logit-link function.

Viral load data were fitted to a GLMM with gravity intensity and radiation level incorporated as fixed orthogonal factors, whereas replicate plates (subjects) and hpi (repeated measures per subject) were both modeled as random factors, a Gamma distribution with a log-link function was used.

Estimated parameters of the model described by Eqs. 1 – 6 were independently fitted to ANOVA models with gravity intensity, radiation level and infection status incorporated as fixed orthogonal factors. Errors were assumed to be Normal.

In all cases, pairwise *post hoc* comparisons were done with the sequential Bonferroni method. The magnitude of the effects was calculated using the η_P^2 statistic, *i.e.*, the proportion of variance in the dependent variable that can be attributed to each model factor after accounting for the variance explained by other factors in the model. Typically, values of $0.06 \leq \eta_P^2 < 0.15$ are considered as medium size effects and $\eta_P^2 \geq 0.15$ are as large magnitude effects.

These analyses were done with SPSS version 29.0.2.0 (IBM Corporation, Armonk, NY)

DATA AVAILABILITY

The datasets generated during the current study are available in the Zenodo respository, https://doi.org/10.5281/zenodo.13869555.

REFERENCES

1. Crucian, B. *et al*. Immune system dysregulation occurs during short duration spaceflight on board the space shuttle. *Journal of Clinical Immunology* **33**, 456–465 (2013).
2. Crucian, B. *et al*. Alterations in adaptive immunity persist during long-duration spaceflight. *npj Microgravity* **1**, 15013 (2015).
3. Bigley, A. B. *et al.* NK cell function is impaired during long-duration spaceflight. *Journal of Applied Physiology* **126**, 842-853 (2019).
4. Agha, N. H. *et al*. Salivary antimicrobial proteins and stress biomarkers are elevated during a 6-month mission to the International Space Station. *Journal of Applied Physiology* **128**, 264-

602 275 (2020).
603 5. Rooney, B. V. B., Crucian, B. E., Pierson, D. L., Laudenslager, M. L. & Mehta, S. K. Herpes
604 virus reactivation in astronauts during spaceflight and its application on Earth. *Frontiers in*
605 *Microbiology* **10**, 16 (2019).
606 6. Mehta, S. K. *et al*. Multiple latent viruses reactivate in astronauts during Space Shuttle
607 missions. *Brain Behavior and Immunity* **41**, 210–217 (2014).
608 7. Mehta, S. K. *et al*. Latent virus reactivation in astronauts on the international space station. *npj*
609 *Microgravity* **3**, 11 (2017).
610 8. Bonomi, G., Checchia, P., D'Errico, M., Pagano, D. & Saracino, G. Applications of cosmic-
611 ray muons. *Progress in Particle and Nuclear Physics* **112**, 103768 (2020).
612 9. Zhao, L. *et al.* The determinant of DNA repair pathway choices in ionizing radiation-induced
613 DNA double-strand breaks. *BMC Research International* **2020**, 4834965 (2020).
614 10. Ceccaldi, R., Rondinelli, B. & D'Andrea, A. D. Repair pathway choices and consequences at
615 the double-strand break. *Trends in Cell Biology* **26**, 52-64.
616 11. Baldwin, J. & Grantham, V. Radiation hormesis: historical and current perspectives. *Journal*
617 *of Nuclear Medicine Technology* **43**, 242–246 (2015).
618 12. Brenner, S. The genetics of *Caenorhabditis elegans*. *Genetics* **77**, 71–94 (1974).
619 13. Kim, W., Underwood, R. S., Greenwald, I. & Shaye, D. D. OrthoList 2: A New comparative
620 genomic analysis of human and *Caenorhabditis elegans* genes. *Genetics* **210**, 445–461 (2018).
621 14. Olsen, A., Vantipalli, M. C. & Lithgow, G. J. Lifespan extension of *Caenorhabditis elegans*
622 following repeated mild hormetic heat treatments. *Biogerontology* **7**, 221–230 (2006).
623 15. Aprison, E. Z. & Ruvinsky, I. Balanced trade-offs between alternative strategies shape the
624 response of *C. elegans* reproduction to chronic heat stress. *PLoS ONE* **9**, e105513 (2014).
625 16. Begasse, M. L., Leaver, M., Vazquez, F., Grill, S. W. & Hyman, A. A. Temperature dependence
626 of cell division timing accounts for a shift in the thermal limits of *C. elegans* and *C. briggsae*.
627 *Cell Reports* **10**, 647–653 (2015).
628 17. Rodriguez, M., Snoek, L. B., Riksen, J. A. G., Bevers, R. P. & Kammenga, J. E. Genetic
629 variation for stress-response hormesis in *C. elegans* lifespan. *Experimental Gerontology* **47**,
630 581–587 (2012).
631 18. Jovic, K. *et al*. Temporal dynamics of gene expression in heat-stressed *Caenorhabditis*
632 *elegans*. *PLoS ONE* **12**, e0189445 (2017).
633 19. Rohlfing, A.K., Miteva, Y., Hannenhalli, S. & Lamitina, T. Genetic and physiological
634 activation of osmosensitive gene expression mimics transcriptional signatures of pathogen
635 infection in *C. elegans*. *PLoS ONE* **5**, e9010 (2010).
636 20. Prithika, U., Deepa, V. & Balamurugan, K. External induction of heat shock stimulates the
637 immune response and longevity of *Caenorhabditis elegans* towards pathogen exposure. *Innate*
638 *Immunity* **22**, 466–478 (2016).

21. Leroy, M., Mosser, T., Manière, X., Alvarez, D. F. & Matic, I. Pathogen-induced *Caenorhabditis elegans* developmental plasticity has a hormetic effect on the resistance to biotic and abiotic stresses. *BMC Evolutionary Biology* **12**, 187 (2012).
22. Castiglioni, V. G. & Elena, S. F. Orsay virus infection increases *Caenorhabditis elegans* resistance to heat-shock. *Biology Letters* **20**, 20240278 (2024).
23. Panek, J. *et al*. A cullin-RING ubiquitin ligase promotes thermotolerance as part of the intracellular pathogen response in *Caenorhabditis elegans*. *Proceedings of the National Academy of Sciences of the USA* **117**, 7950–7960 (2020).
24. De Souza, E. A., Thompson, M. A. & Taylor, R. C. Olfactory chemosensation extends lifespan through TGF-β signaling and UPR activation. *Nature Aging* **3**, 938-947 (2023).
25. Le Pen, J. *et al*. Terminal uridylyltransferases target RNA viruses as part of the innate immune system. *Nature Structural Molecular Biology* **25**, 778-786.
26. Ashe, A. *et al*. A deletion polymorphism in the *Caenorhabditis elegans* RIG-I homolog disables viral RNA dicing and antiviral immunity. *eLife* **2**, e00994 (2013).
27. Félix, M.A. *et al*. Natural and experimental infection of *Caenorhabditis* nematodes by novel viruses related to nodaviruses. *PLoS Biology* **9**, e1000586 (2011).
28. Huang, Y. *et al*. Heat stress reduces the susceptibility of *Caenorhabditis elegans* to Orsay virus infection. *Genes* **12**, 1161 (2021).
29. Van Voorhies, W. A., Castillo, H. A., Thawng, C. N. & Smith, G. B. The phenotypic and transcriptomic response of the *Caenorhabditis elegans* nematode to background and below-background radiation levels. *Frontiers in Public Health* **8**, 581796 (2020).
30. Morciano, P. *et al*. Effects of reduced natural background radiation on *Drosophila melanogaster* growth and development as revealed by the FLYINGLOW program. *Journal of Cellular Physiology* **233**, 23–29 (2018).
31. Tee, L. F. *et al.* Effects of simulated microgravity on gene expression and biological phenotypes of a single generation *Caenorhabditis elegans* cultured on 2 different media. *Life Sciences in Space Research* **15**, 11–17 (2017).
32. Liu, H., Guo, D., Kong, Y., Rui, Q. & Wang, D. Damage on functional state of intestinal barrier by microgravity stress in nematode *Caenorhabditis elegans*. *Ecotoxicology and Environmental Safety* **183**, 109554 (2019).
33. Zhao, L., Rui, Q. & Wang, D. Molecular basis for oxidative stress induced by simulated microgravity in nematode *Caenorhabditis elegans*. *Science of the Total Environment* **607–608**, 1381–1390 (2017).
34. Zhou, Y., Chen, H., Zhong, W. & Tao, Y. J. Collagen and actin network mediate antiviral immunity against Orsay virus in *C. elegans* intestinal cells. *PLoS Pathogens* **20**, e1011366 (2024).
35. Johnstone, I. L. Cuticle collagen genes. Expression in *Caenorhabditis elegans*. *Trends in*

Genetics **16**, 21-27.

36. Castiglioni, V. G. *et al*. Story of an infection: viral dynamics and host responses in the *Caenorhabditis elegans*-Orsay virus pathosystem. *Science Advances* **10**, eadn5945 (2024).
37. Goswami, P. C., Roti Roti, J. L. & Hunt, C. R. The cell cycle-couple expression of topoisomerase IIα during S phase is regulated by mRNA stability and is disrupted by heat shock or ionizing radiation. *Molecular and Cellular Biology* **16**, 1500-1508 (1996).
38. Morran, L. T., Cappy, B. J., Anderson, J. L. & Phillips, P. C. Sexual partners for the stressed: facultative outcrossing in the self-fertilizing nematode *Caenorhabditis elegans*. *Evolution* **63**, 1473-1482 (2009).
39. Slowinski, S. P. *et al*. Outcrossing in *Caenorhabditis elegans* increases in response to food limitation. *Ecology and Evolution* **14**, e11166 (2024).
40. Lv, H. *et al*. Microgravity and immune cells. *Journal of the Royal Society Interface* **20**, 20220869 (2023).
41. Willis, C. R. G. *et al*. Comparative transcriptomics identifies neuronal and metabolic adaptations to hypergravity and microgravity in *Caenorhabditis elegans. iScience* **23**, 101734 (2020).
42. Çelen, I., Jayasinghe, A., Doh, J. H. & Sabanayagam, C. R. Transcriptomic signature of the simulated microgravity response in *Caenorhabditis elegans* and comparison to spaceflight experiments. *Cells* **12**, 270 (2023).
43. Duxbury, E. M. L. *et al*. Reduced insulin/IGF-1 signalling upregulates two anti-viral immune pathways, decreases viral load and increases survival under viral infection in *C. elegans*. *GeroScience* https://doi.org/10.1007/s11357-024-01147-7 (2024).
44. Van der Hoeven, R., McCallum, K. C., Cruz, M. R. & Garsin, D. A. Ce-Duox1/BLI-3 generated reactive oxygen species trigger protective SKN-1 activity via p39 MAPK signaling during infection in *C. elegans*. *PLoS Pathogens* **7**, e1002453 (2011).
45. L'Hernault, W. E. Spermatogenesis. In: Riddle, D. L. (ed). *C. elegans II*. Cold Spring Harbor, NY: Cold Spring Harbor Laboratory Press (1997). pp. 271-94.
46. McGovern, M., Yu, L., Kosinski, M., Greenstein, D. & Savage-Dunn, C. A role for sperm in regulation of egg-laying in the nematode *C. elegans*. *BMC Developmental Biology* **7**, 41 (2007).
47. Kuwabara, P. E. The multifaceted *C. elegans* major sperm protein: an ephrin signaling antagonist in oocyte maturation. *Genes Development* **17**, 155-161 (2003).
48. Bakowski, M. A. *et al.* Ubiquitin-mediated response to microsporidia and virus infection in *C. elegans*. *PLoS Pathogens* **10**, e1004200 (2014).
49. Trzaska, W. H., *et al*. Cosmic-ray muon flux at Canfranc Underground Laboratory. *European Physical Journal C* **79**, 721 (2019).
50. Workman, R. L. *et al*. The review of particle physics. *Progress in Theoretical and*

Experimental Physics **2022**, 083C01 (2022).
51. Castiglioni, V. G., *et al*. Experimental evolution of an RNA virus in *Caenorhabditis elegans*. *Infection Genetics and Evolution* **123**, 105623 (2024).
52. Schindelin, J., *et al*. Fiji: an open-source platform for biological-image analysis. *Nature Methods* **9**, 676-682 (2012).
53. Kissoyan, K. A. B., *et al.* Natural *C. elegans* microbiota protects against infection via production of a cyclic lipopeptide of the viscosin group. *Current Biology* **29**, 1030-1037.e5 (2019).
54. Balaguer, F., *et al*. *Bifidobacterium animalis* subsp. *lactis* BPL1™ and its lipoteichoic acid modulate longevity and improve age/stress-related behaviors in *Caenorhabditis elegans*. *Antioxidants* **12**, 2107 (2023).

ACKNOWLEDGEMENTS

We thank Francisca de la Iglesia (I2SysBio) and Rebecca Hernández (LSC) for excellent technical support. We are deeply grateful to Carlos P. Garay (LSC) for his commitment and dedication to research in subterranean biology, as well as his constant material and emotional support. Many computations were performed on the HPC cluster Garnatxa at I2SysBio (CSIC-UV). This study was supported by ESA contract 4000135960/21/NL/GLC/my, grant PID2022-136912NB-I00 funded by MCIN/AEI/10.13039/501100011033 and by "ERDF a way of making Europe", grant CIPROM/2022/59 funded by Generalitat Valenciana, and grant PB-02-22 from ICTS Laboratorio Subterráneo de Canfranc to S.F.E. V.G.C. was supported by grant FJC2021-047264-I funded by MCIN/AEI/10.13039/501100011033 and by NextGenerationEU/PRTR. E.G.L. was supported by grant FPU21/00410 funded by MCIN/AEI/10.13039/501100011033 and by "ESF invest in your future". J.C.M-S. was supported by grant ACIF/2021/296 from Generalitat Valenciana. The funders played no role in study design, data collection, analysis and interpretation of data, or the writing of this manuscript.

AUTHOR CONTRIBUTIONS

AVG, VGC and EGL performed the experiments; VGC and SFE supervised the experimental work; AVG, RG, VGC, and SFE conceived and designed the experiments; AVG and SFE analyzed the data; AVG and SFE wrote the paper; AVG, VGC, EGL, RG, and SFE edited and approved the final version.

COMPETING INTERESTS

The authors declare no financial or non-financial competing interests.

ADDITIONAL INFORMATION

Supplementary information The online version contains supplementary material available at https://doi.org/.

Correspondence and requests for materials should be addressed to Santiago F. Elena.

Table 1. Results of the fecundity data fitting to the GLMM testing for the effect of gravity intensity, muon radiation flux and OrV infection. Significant effects of small magnitude are highlighted in light gray, while significant effects of medium and large magnitude are highlighted in dark gray.

		Unfertilized eggs (*U*)			**Nonviable embryos (*N*)**			**Progeny (*A*)**			**Reproductive success (*R*)**		
Source of variation	**d.f.**	F	P	η_P^2	F	P	η_P^2	F	P	η_P^2	F	P	η_P^2
Model	7, 592	3.113	0.003	0.036	11.702	< 0.001	0.122	13.129	< 0.001	0.134	19.737	< 0.001	0.189
Gravity intensity	1, 592	1.923	0.166	0.003	3.825	0.051	0.006	22.538	< 0.001	0.037	13.221	< 0.001	0.022
Muon radiation flux	1, 592	1.122	0.290	0.002	5.010	0.026	0.008	0.410	0.522	0.001	0.425	0.515	0.001
Infection status	1, 592	3.864	0.050	0.006	9.244	0.002	0.015	19.131	< 0.001	0.031	47.457	< 0.001	0.074
Gravity × Radiation	1, 592	1.866	0.172	0.003	23.054	< 0.001	0.037	21.024	< 0.001	0.034	9.599	0.002	0.016
Gravity × Infection	1, 592	1.968	0.161	0.003	12.585	< 0.001	0.021	13.209	< 0.001	0.022	14.810	< 0.001	0.024
Radiation × Infection	1, 592	1.624	0.203	0.003	15.129	< 0.001	0.025	1.097	0.295	0.002	8.321	0.004	0.014
Gravity × Radiation × Infection	1, 592	2.020	0.156	0.003	0.259	0.611	0.000	6.689	0.010	0.011	10.964	< 0.001	0.018

Table 2. Estimation of model parameters and initial condition. Values represent the mean of the replicates (±1 SD). See Fig. S2 for the fitting to the experimental data.

Gravity intensity	Muon radiation flux	Infection status	G_0	α	δ (d^{-1})	η (d^{-1})	γ	μ
Standard	Standard	non-inoculated	252.773 ±32.217	0.936 ±0.011	0.891 ±0.215	0.584 ±0.235	0.015 ±0.011	0.989 ±0.003
Standard	Standard	inoculated	303.236 ±113.438	0.912 ±0.129	0.543 ±0.126	1.199 ±0.497	0.004 ±0.005	0.988 ±0.005
μG	Standard	non-inoculated	277.392 ±21.302	0.938 ±0.049	0.667 ±0.166	0.659 ±0.103	0.004 ±0.003	0.986 ±0.014
μG	Standard	inoculated	292.661 ±84.967	0.824 ±0.100	0.486 ±0.138	1.242 ±0.329	0.029 ±0.036	0.970 ±0.028
Standard	BBR	non-inoculated	293.401 ±27.615	0.924 ±0.068	0.416 ±0.072	0.676 ±0.220	0.013 ±0.020	0.974 ±0.008
Standard	BBR	inoculated	356.747 ±66.461	0.844 ±0.105	0.417 ±0.075	0.764 ±0.282	0.019 ±0.019	0.983 ±0.012
μG	BBR	non-inoculated	257.598 ±65.897	0.888 ±0.095	0.495 ±0.084	0.689 ±0.438	0.012 ±0.018	0.978 ±0.015
μG	BBR	inoculated	283.136 ±57.662	0.853 ±0.103	0.451 ±0.128	0.641 ±0.197	0.028 ±0.033	0.975 ±0.014

G_0: Germline precursor cells at $t = 0$; α: germline precursor cells to spermatocytes initial ratio; δ: rate of germline precursor cells differentiation into mature oocytes; η: rate of oocytes migration from the distal gonads to the spermathecae; γ: scale parameter of the fecundation efficiency function; μ: fraction of a fecundated eggs developing into an L1 larvae ($1 - \mu$ would be the fraction of a fecundated eggs which abort its development).

761